

## Shearing characteristics of slip zone soils and strain localization analysis of a landslide

Dong Liu<sup>a</sup> and Xiaoping Chen<sup>\*</sup>

MOE Key Laboratory of Disaster Forecast and Control in Engineering,  
College of Science and Engineering, Jinan University, Guangzhou, 510632, PR China

(Received January 17, 2013, Revised August 16, 2014, Accepted September 01, 2014)

**Abstract.** Based on the Mohr-Coulomb failure criterion, a gradient-dependent plastic model that considers the strain-softening behavior is presented in this study. Both triaxial shear tests on conventional specimen and pre-cut-specimen, which were obtained from an ancient landslide, are performed to plot the post-peak stress-strain entire-process curves. According to the test results of the soil strength, which reduces from peak to residual strength, the Mohr-Coulomb criterion that considers strain-softening under gradient plastic theory is deduced, where strength reduction depends on the hardening parameter and the Laplacian thereof. The validity of the model is evaluated by the simulation of the results of triaxial shear test, and the computed and measured curves are consistent and independent of the adopted mesh. Finally, a progressive failure of the ancient landslide, which was triggered by slide of the toe, is simulated using this model, and the effects of the strain-softening process on the landslide stability are discussed.

**Keywords:** gradient plastic theory; triaxial shear test; landslide; strain localization; progressive failure

### 1. Introduction

The stability analysis of slopes in soils with strain-softening behavior is a notably complex problem. The strength of these strain-softening materials reduces from peak to residual strength when they were affected by the loads, and a severe deformation shear zone is formed because of the local stress concentration, which is commonly called strain localization. Considering that the strain localization problem is strain-dependent, it will be difficult to solve the stability problem of slopes in soils with strain-softening by adopting the traditional limit equilibrium method. To simulate the formation and development of shear zones where the strain localizes, numerical solutions based on the finite-element method are frequently used. The finite-element method was used by several authors to analyze the stability of slopes with strain-softening behavior (Skempton 1964, Bjerrum 1967, Chen *et al.* 1992, Mohammadi and Taiebat 2013). Great contributions were made by Potts and his coworkers, who monitored and analyzed the failure of some embankments in the long term (Dounias *et al.* 1988, Potts *et al.* 1990, Georiadis *et al.* 2004). In these studies, an elasto-plastic constitutive model using the Mohr-Coulomb yield criterion was proposed, and the

---

\*Corresponding author, Professor, E-mail: [chenxp@jnu.edu.cn](mailto:chenxp@jnu.edu.cn)

<sup>a</sup> Ph.D., E-mail: [liudong04@126.com](mailto:liudong04@126.com)

strain-softening character was reflected when the strength parameters were reduced with the increasing deviatoric plastic strain. In other studies, some difficulties were found when the finite-element method was adopted to capture the development of the shear zone, such as numerical instabilities and mesh dependence (Pietruszczak and Mroz 1981, Brinkgreve 1994, Lu and Yang 2013). Therefore, simulating the failure of slopes in soils with strain-softening behavior deserves particular attention; otherwise, the calculation may be stopped by the divergence, which is caused by the lack of convergence. In addition, a model simulation may have different results when different mesh densities are adopted. To overcome these drawbacks, some improved constitutive models were proposed, such as the Cosserat model (De Brost 1991, De Brost and Sluys 1991), strong discontinuity model (Simo and Oliver 1993), and other models based on the gradient and non-local theories (Di Prisco *et al.* 2002, Di Prisco and Imposimato 2003). A proper approach to alleviate the mesh dependence is to use the non-local elasto-viscoplastic model, where the strain-softening behavior is simulated by reducing the strength parameters with the accumulated deviatoric plastic strains (Troncone 2005, Han *et al.* 2013, Conte *et al.* 2010, 2013). In particular, De Brost formulated a plasticity-dependent model where the yield strength depends on an equivalent plastic strain measure and the Laplacian thereof (De Brost 1992, De Brost and Pamin 1996). This approach was developed by Chen *et al.* (1992) (Wang *et al.* 2004) and successively extended by other authors (Chen and Baker 2004a, b, Lars and Stergios 2009). In the latest studies, the hardening modulus that was used in the numerical approach based on the gradient and non-local theories is always considered invariant, which simplifies the calculation. However, because the hardening modulus continuously varies with the reduction of the strength parameter of the soils, it is not strictly consistent with the physical truth.

In the present study, a gradient-dependent plastic model that considers the strain-softening behavior is proposed. The strain-softening characteristic of the slip-zone soils from an ancient landslide was obtained by carrying out a series of triaxial shear tests on conventional specimens and precut specimens. The model uses the Mohr-Coulomb yield function under the guidance of the gradient-dependent plastic theory, and the strength parameters are reduced with the equivalent plastic strain. In particular, the strength reduction depends on the hardening parameter and the Laplacian thereof, and the numerical approach based on the model has a constantly changing hardening modulus, which is precisely obtained from the strength reduction curves. Some engineering applications of the model are shown. The model is imposed to simulate the process of the triaxial shear test, and the results of the numerical calculation with different mesh densities are compared with the measured value of the triaxial shear test. Moreover, a numerical approach based on the model is performed for the progressive failure of landslide in soils with strain-softening behavior.

## 2. The drained triaxial shear behavior of slip zone soils

### 2.1 Nature of the investigated slip zone soil

The samples in this study were collected from an ancient slip zone, which was located in Shaoguan City in the Guangdong province of China and had a soil volume of approximately 2,400,000 m<sup>3</sup> (see Figs. 1 and 2). Fig. 2 demonstrated soil specimens from the ancient landslide, which were obtained by drilling exploration. Since the landslide is near the Lechangxia Reservoir, its reactivated potential has been given much attention.



Fig. 1 Geographic location of the ancient landslide



Fig. 2 Specimen taken from the ancient landslide

Table 1 Soil parameters (Chen *et al.* 2011b)

Water content $w/\%$	Bulk density $\rho/g.cm^{-3}$	Void ratio $e$	Liquid limit $w_L/\%$	Plastic limit $w_P/\%$	Plasticity index $I_P$	Liquidity index $I_L$	Optimum water content $w_{op}/\%$	Maximum dry density $\rho_{dmax}/g.cm^{-3}$	Permeability coefficient $k_v/cm/s$
16.0	2.08	0.567	29	16.8	12.2	-0.06	12.7	1.87	$4.78 \times 10^{-4} \sim 1.60 \times 10^{-7}$

The slip zone, which contained crushed clayed sandstone and silty sandstone, was between the landslide body and the bed rock and was categorized as clays with sand with low-liquid-limit soils in previous studies (Chen *et al.* 2011b). The properties and the particle size distribution are summarized in Table 1 and Fig. 3.

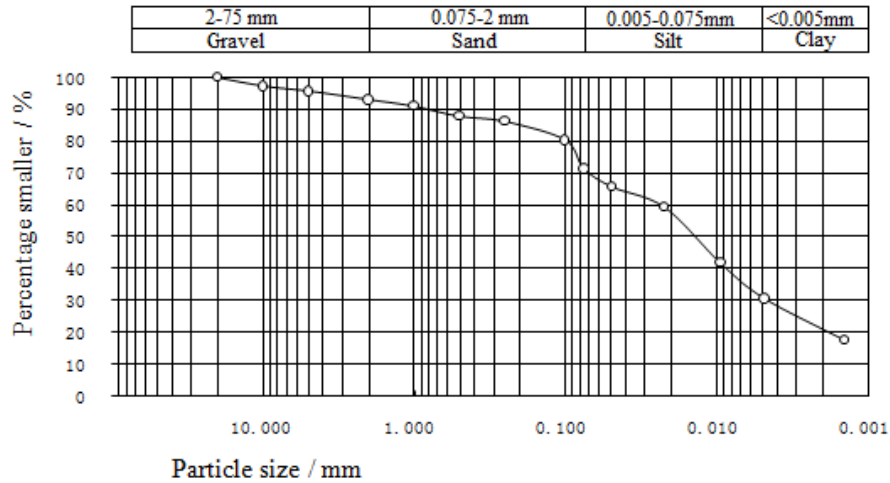


Fig. 3 Particle size distribution curve (Chen *et al.* 2011b)

## 2.2 Test method and test scheme

The drained triaxial shear tests were performed on the conventional specimens and precut specimens (Chinese National Standard 2001). The conventional specimen was cylindrical with a diameter length of 39.1 mm and a height of 80 mm (Fig. 4(a)). The precut specimen was identical in size with the conventional specimen, but it was wire cut to form a shear plane before the test began to concentrate the shear displacement along a well-defined failure plane (Fig. 4(b)). The specimen was pretreated by cutting a plane according to the failure angle  $\theta$ , which is a theoretical angle between the major principal plane and the failure plane, which is relevant to the friction angle  $\varphi$  (generally take  $45^\circ + \varphi / 2$ ). This cut increased the likelihood that the residual strength would be quickly obtained before the maximum permissible shear displacement was attained in the triaxial device. The triaxial test in the paper was a Consolidated Drained test, where the pore water pressure in the entire shear process remained zero at a notably low shear rate, and the conventional specimens and wire cut specimens were all initially saturated before the shearing tests. The wire-cut specimens were pretreated by cutting a plane with a hairline wire, the cut-plane should be as thin as possible (such as the maximum particle size), and the roughness of the cut



(a) Specimen in TRD test



(b) Specimen in PTRD test

Fig. 4 Two types of specimen

plane was carefully controlled to be exactly similar to a naturally formed cut plane by notably slightly cutting with the hairline wire. The triaxial shear test with the conventional specimen is called the TRD test for short in this paper, and the test with the precut-specimen is called the PTRD test. The shear rate of the two tests was 0.0072 mm/min, and the specimen in the two tests had identical water content and density for comparison purposes. The applied all-round pressure for the two tests was 50, 100, and 200 kPa. All properties of the specimens are summarized in Table 2.

### 2.3 Test results and discussion

The specimens after the tests are shown in Fig. 5, and the strength envelope curves are displayed in Fig. 6. The failure envelopes in Fig. 6 were fitted using the stress values from the two tests. The upper failure envelopes were fitted using the peak stress value from the TRD test, while the lower failure envelopes were fitted using the minimum constant stress value from the PTRD test. Since the specimens in the two tests had identical water content and density, and they were all initially saturated before the two shearing tests started, the different failure envelopes from the two tests were attributed to the precutting condition. The specimens after the TRD test experienced a drum-shaped deformation (Fig. 5(a)), and the shear zone didn't appear because of the shear displacement limit. The peak in this test can be defined as the peak strength, which has cohesion intercept  $c = 10$  kPa and internal friction angle  $\varphi = 29.3^\circ$  (Fig. 6). Unlike the specimens after the TRD test, the specimens after the PTRD test show a shearing plane and a shear zone (Fig. 5(b)).

Table 2 Properties of the specimens

Test	Water content (%)	Void ratio	Bulk density (g/cm <sup>3</sup> )	All-round pressure (kPa)
TRD1	16.0	0.57	2.08	50
TRD2	15.9	0.59	2.07	50
TRD3	16.1	0.55	2.09	50
TRD4	15.8	0.61	2.08	100
TRD5	15.7	0.60	2.06	100
TRD6	16.0	0.57	2.10	100
TRD7	15.9	0.58	2.09	200
TRD8	16.2	0.57	2.08	200
TRD9	16.1	0.60	2.06	200
PTRD1	15.8	0.54	2.07	50
PTRD2	16.2	0.55	2.08	50
PTRD3	16.0	0.57	2.09	50
PTRD4	16.3	0.58	2.10	100
PTRD5	16.2	0.57	2.07	100
PTRD6	16.1	0.59	2.08	100
PTRD7	15.8	0.58	2.06	200
PTRD8	15.9	0.61	2.07	200
PTRD9	16.0	0.59	2.09	200



Fig. 5 Specimen after test

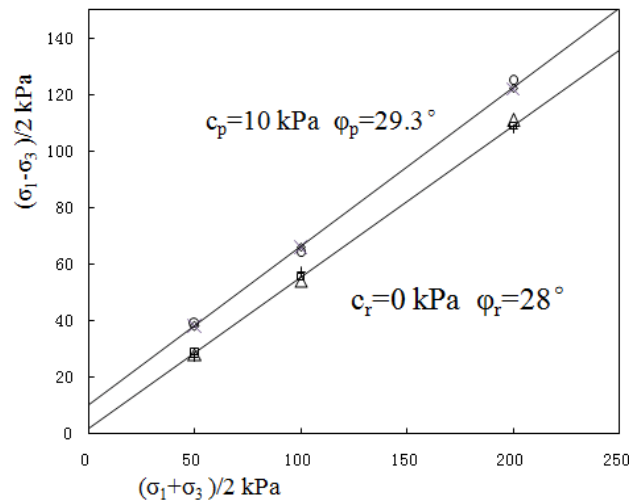


Fig. 6 Strength envelopes of tests

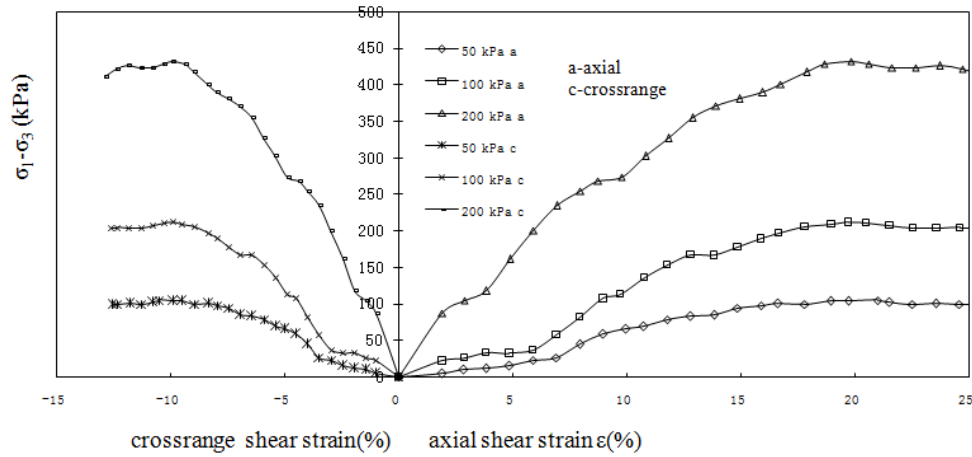
The minimum constant value in this test can be defined as residual strength, which has  $c = 0 \text{ kPa}$  and  $\phi = 28^\circ$  (Fig. 6). All shear strength parameters in this paper were obtained from the Consolidated Drained triaxial test, the pore water pressure in the entire shear process remained zero or a small value, so all shear strength parameters in the paper were effective parameters. Compared the peak and the residual strength of the slip zone soil, the internal friction angle slightly decreases, but the cohesion intercept decreases to almost zero.

The results of the TRD test (Fig. 7(a)) show that as the strain limit of the shear apparatus, the maximum axial strain can commonly only reach 25%, and the corresponding cross-range shear strain is approximately 15%. Since the slip-zone soil requires a larger shear displacement to reach the residual state, the shear apparatus cannot satisfy the requirements. Because of the disadvantage, the entire process curves that reflect strain-softening cannot be obtained by the test.

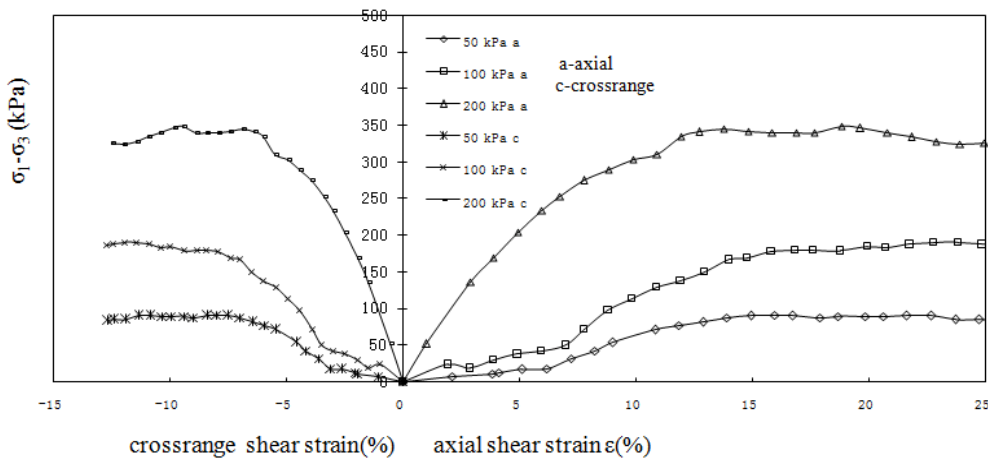
The PTRD test (Fig. 7(b)) demonstrated that similar to the TRD test, the deviator stress increases when the strain grows in the earlier stage of the PTRD test, but the deviator stress quickly reaches a peak value which is lower than the peak value of the TRD test. In the later stage, the deviator stress began to stabilize and finally reached a residual value.

To compare the two tests, the results are put together in Fig. 8. Although the earlier stage of the

two tests is similar, the peak value of the deviator stress in the TRD test is obviously higher than that of the PTRD test, and the TRD test costs more time to reach the peak value than the PTRD test. The phenomenon is more obvious when the all-round pressure increased. Considering that the specimen of the PTRD test has a precut plane, it is easier to reach the residual strength because the shear displacement has been notably enlarged. The deviator value of the PTRD test in the later stage can be considered as a stable value, so it is a good approach to obtain the residual strength from the PTRD test. Assuming that the specimens of the two tests have identical water content and density, the test conditions of the two tests are identical; thus, the peak value of the deviator stress in the TRD test is higher than that in the PTRD test because the PTRD test is a shear test on precut specimens, which implies that the PTRD test starts at specimens with shear zones without the peak shear process. This method proves useful in obtaining the residual strength rather than the peak strength value. The TRD test is a test on intact specimens, which implies that the TRD test starts



(a) TRD test



(b) PTRD test

Fig. 7 Stress-strain curve

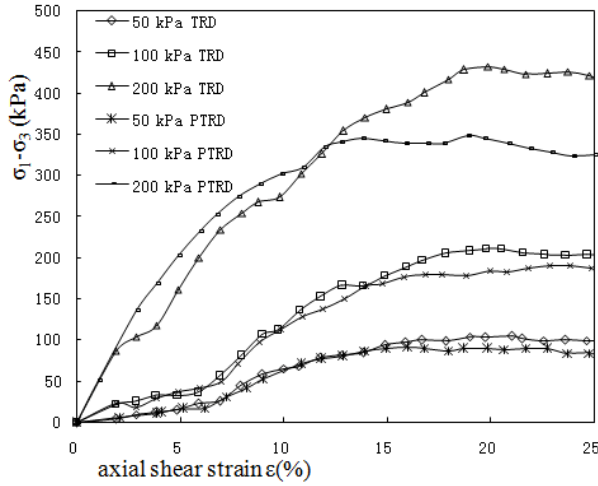


Fig. 8 Comparison of two tests

from zero strain, and the peak strength can be obtained as a result. Thus, the difference of the starting shear process is the main cause of the difference in peak strength value of the two tests.

It can be presumed that in the last stage of the TRD test, if the shear continues, the deviator stress should continually reduce until a stable residual value is attained, and the residual value should be almost identical to the residual value of the PTRD test because the water content and density of the specimen in the two tests are identical. However, the shear was disturbed because the shear displacement is limited. Hence, the stress-strain curve of the TRD test is incomplete. Considering that the specimen of the PTRD test slipped along the precut plane, the deviator stress quickly reached the peak value, and a stable residual value can be easily obtained. However, the earlier stage of the PTRD test curve of a precut specimen is unavailable because it cannot represent the real mechanical model. Thus, the stress-strain curve of the PTRD test is also incomplete.

Slope failure always occurs resulting from the soil strength reduction with increasing strain. To clarify the mechanism of the slope failure and realize the strain-softening characteristics of the

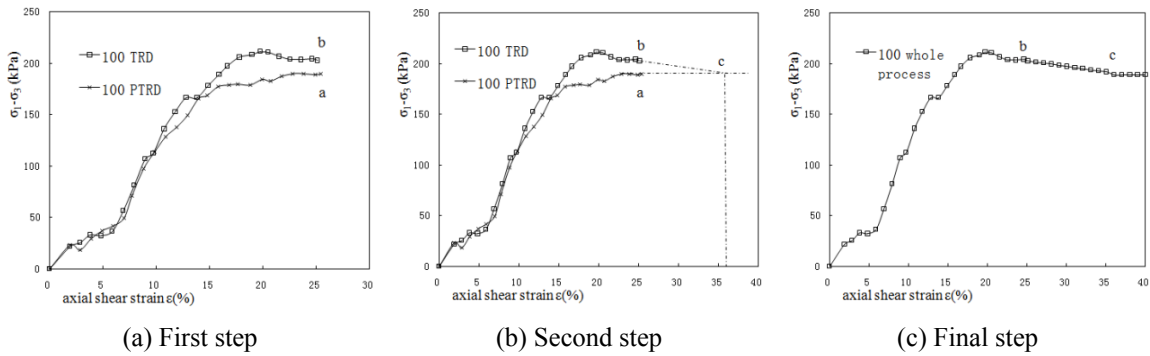


Fig. 9 Steps to obtain the strain-softening of the entire process

soil, the strain-softening of the entire process must be studied. Two different tests can be synthesized to obtain the strain-softening of the entire process and hence a method was proposed in the present study (for example, all-round pressure  $p = 100$  kPa, see Fig. 9): (a) putting the two stress-strain curves in the same coordinate system, where the ends of the two curves are points a and b; (b) drawing the asymptote of the stress-strain curves of the PTRD test from point a, then extending the trend line of the stress-strain curves of the TRD test from point b, and an intersection point c can be obtained; (c) connecting points b and c in line and horizontally extending the curve. The entire process of the drained triaxial shear stress-axial strain relationship is shown in Fig. 10, which shows the complete strain-softening characteristics of slip zone soils.

### 3. Gradient-dependent plastic model considering the strain-softening behavior

#### 3.1 The post-peak decrease of the strength parameters

Based on the stress-strain relationship in Fig. 10, the variation of the strength parameters is proposed. Suppose that the soil and the strain-softening characteristic are isotropic. The equivalent plastic strain  $\varepsilon_{ep}$  is considered the hardening parameter  $\kappa$ , which is defined as

$$\dot{\kappa} = \varepsilon_{ep} = \sqrt{\frac{2}{3} [(\varepsilon_1^p - \varepsilon_2^p)^2 + (\varepsilon_2^p - \varepsilon_3^p)^2 + (\varepsilon_3^p - \varepsilon_1^p)^2]} \quad (1)$$

where  $\varepsilon_{ij}^p$  is the plastic deformation tensor.

The yield function is expressed as follows

$$f(\sigma_1, \sigma_2, \sigma_3, \varepsilon_{ep}) = 0 \quad (2)$$

where  $\sigma_i$  denotes the stress components.

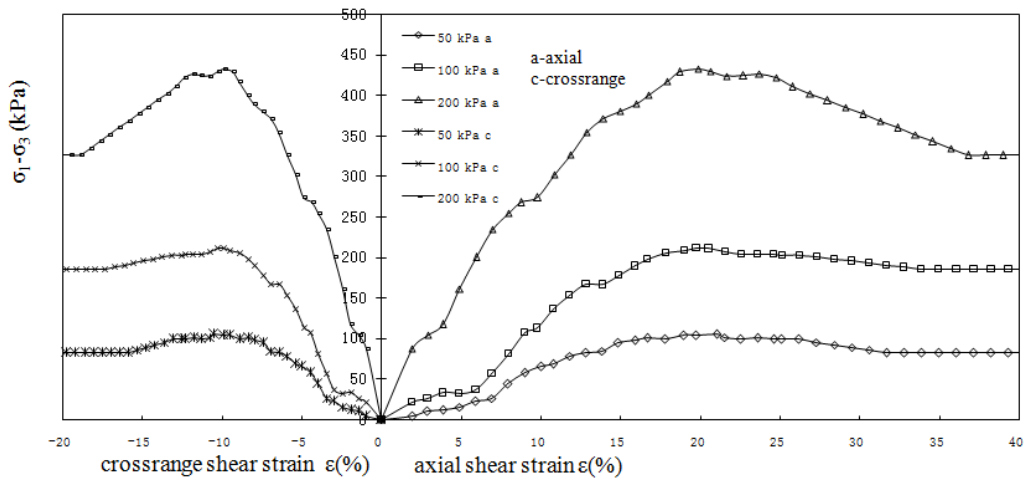


Fig. 10 Drained triaxial shear entire-process curves of slip zone soil

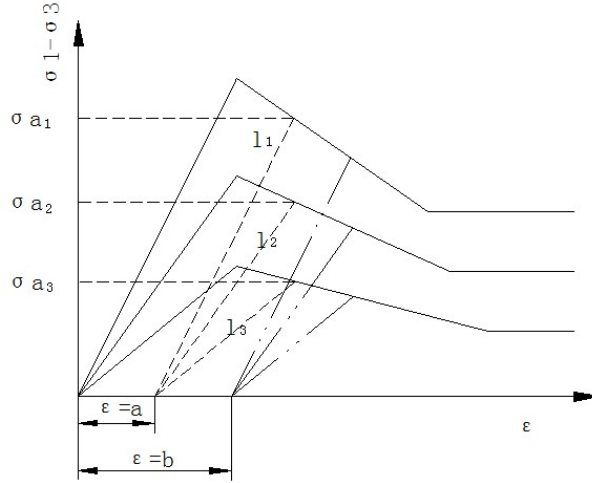


Fig. 11 Simplified stress-strain curve

The relationship of the deviator stress  $\sigma_1 - \sigma_3$  with the axial strain  $\varepsilon_1$  and the cross-range strain  $\varepsilon_3$  can be obtained from the entire-process curve (see Fig. 10).

By simplification, the entire-process curve in Fig. 10 can be expressed as three segment lines with different slopes (Fig. 11): ascent stage, descent stage and residual stage. Assuming that the unloading curve has the same slope as the ascent stage of loading curves, when the plastic strain  $\varepsilon = a$ , the yield stress can be obtained from the unloading line  $l_i$  ( $i = 1, 2, 3$ ), which represents different all-round pressures. Fig. 11 shows that the yield stresses are  $\sigma_{a1}, \sigma_{a2}, \sigma_{a3}$  under different all-round pressures when the plastic strain  $\varepsilon = a$ . The yield stress with other plastic strains under different all-round pressures can be similarly obtained (for example, strain = b).

Furthermore, assume that the initial yield and the subsequent yield follow Mohr-Coulomb yield function. The yield function can be matched as

$$f = \sigma_1 - k\sigma_3 + m \quad (3)$$

where  $k$  and  $m$  are coefficients

$$k = (1 + \sin \varphi) / (1 - \sin \varphi) \quad (4)$$

$$m = (2c \cos \varphi) / (1 - \sin \varphi) \quad (5)$$

The practical significance of Fig. 10 and Eq. (3) is: when a plastic strain occurs, the corresponding yield stress can be determined using Fig. 10; then, the strength parameters can be obtained using Eq. (3) and the formulas of  $k$  and  $m$ . For example, when  $\varepsilon_{ep} = 0.2$ , the yield stress is listed in Table 3, and it can be derived that  $k = 2.8$  and  $m = 13.6$ . Then, from Eqs. (4)-(5),  $c = 4$  and  $\varphi = 28.3^\circ$ . Using the same methods, the strength parameters with different equivalent plastic strains can be obtained. Fig. 12 gives the relationship of strength reduction of the slip zone soils with increasing equivalent plastic strains.

Table 3 Yield stresses under different all-round pressures when  $\varepsilon_{ep} = 0.2$

All-round pressures/kPa	50	100	200
Yield stress/kPa	81	176	365

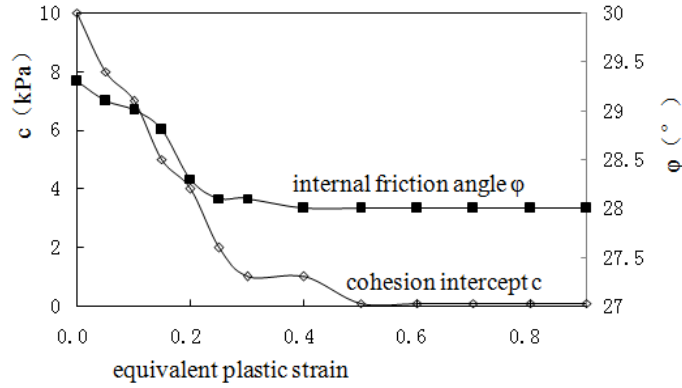


Fig. 12 Strength reduction with strain

### 3.2 Mohr-Coulomb model with strain softening based on the gradient-dependent plastic theory

When the finite-element method is adopted, classical elastic-plastic models with strain-softening often result in numerical instabilities and mesh dependence, which often makes the numerical calculation abort. To solve the problem, the gradient-dependent plasticity theory is proposed, where the yield strength depends on the hardening parameter and the Laplacian thereof. The theory has been developed by several authors (De Borst 1992, Wang *et al.* 2001), and some numerical examples using the gradient-type model have shown that the solution does not exhibit the pathological mesh-dependence.

The Mohr-coulomb yield function has been widely used in soil mechanics as follows

$$F = \frac{1}{3} I_1 \sin \varphi + \left( \cos \theta_\sigma - \frac{1}{\sqrt{3}} \sin \theta_\sigma \sin \varphi \right) \sqrt{J_2} - \cos \varphi c = 0 \tag{6}$$

where

$$I_1 = (\sigma_1 + \sigma_2 + \sigma_3) / 3 \tag{7}$$

$$J_2^2 = [(\sigma_1 - \sigma_2)^2 + (\sigma_2 - \sigma_3)^2 + (\sigma_3 - \sigma_2)^2] / 6 \tag{8}$$

$\theta_\sigma$  is the lode angle,  $c$  and  $\varphi$  are the strength parameters.

Assuming that the lode angle  $\theta_\sigma = 0$ , the Mohr-coulomb yield function can be written in the  $p$ - $q$  surface as

$$F = \frac{\sqrt{3}}{3 \cos \varphi} q - p \tan \varphi - c \tag{9}$$

where

$$p = \frac{1}{3}I_1 \quad (10)$$

$$q = \sqrt{3J_2} \quad (11)$$

Assuming that the softening behavior indicates that the cohesion intercept  $c$  can reduce, and the reduction depends on the hardening parameter and the Laplacian thereof

$$F = \frac{\sqrt{3}}{3\cos\varphi}q - p \tan\varphi - (c + h\dot{\kappa} + hl^2\dot{\kappa}) \quad (12)$$

Where the hardening modulus  $h$  is defined as in classical mechanics

$$h = -\frac{1}{\dot{\lambda}} \frac{\partial f}{\partial \kappa} \dot{\kappa} \quad (13)$$

$\dot{\lambda}$  is a non-negative scalar-valued quantity, which measures the plastic flow intensity.

$l$  is defined as the characteristic length and has a dimension of length.

The equivalent plastic strain  $\varepsilon_{ep}$  is considered the hardening parameter  $\dot{\kappa}$ , which is expressed in Eq. (1)

Generally, a relationship can be established between  $\dot{\lambda}$  and  $\dot{\kappa}$

$$\dot{\kappa} = \eta \dot{\lambda} \quad (14)$$

where  $\eta$  is a constant.

For the Mohr-Coulomb yield function, it is shown in this study that

$$\eta = \sqrt{\frac{3 + 2\sin^2\varphi}{9\cos^2\varphi}} \quad (15)$$

Thus, the yield function can be written as

$$f(\sigma, \lambda, \nabla^2 \lambda) = 0 \quad (16)$$

where  $\sigma$  is a vector that contains the stress components ( $\sigma_{xx}, \sigma_{yy}, \sigma_{zz}, \sigma_{xy}, \sigma_{yz}, \sigma_{zx}$ ).

A gradient-dependent plastic soil model that considers the strain-softening behavior is adopted in this study. The model takes the Mohr-Coulomb yield criterion as the yield function where the yield strength depends on the hardening parameter and the Laplacian thereof.

### 3.3 Model parameters

For the traditional Mohr-Coulomb model, the required soil parameters in the calculations are: Young's modulus  $E$ , Poisson's ratio  $\nu$ , and strength parameters  $c$  and  $\varphi$ . For models based on the gradient-dependent plastic theory, more parameters are required (De Borst 1992, Wang *et al.* 2001,

Chen 2004a, b): the characteristic length  $l$  and the hardening modulus  $h$ , which are usually adopted as constants.

In this study, all adopted parameters can be obtained from the strain-softening entire-process curve, which is previously introduced in the present study (Figs. 10 and 12). In particular, the cohesion intercept  $c$  varies with the equivalent plastic strain, which depends on the hardening parameter and the Laplacian thereof ( $c' = c + h\dot{\kappa} + hl^2\ddot{\kappa}$ ). Based on the reduction relationship of the strength parameters with the equivalent plastic strain (Fig. 12), the slope of the curve can be considered as the hardening modulus  $h$ .

The characteristic length  $l$  adopts a constant value, which is identical to the previous study. The hardening modulus, which is considered as the slope of the strain-softening entire-process curve, can be obtained from the curve as a dynamic changing value. Thus, the parameters of the gradient-dependent plastic soil model based on the strain-softening of the entire process are more precise and more strictly conforming to the physical truth.

### 3.4 Numerical verification of the model

The triaxial shear test is simulated to verify the gradient-dependent plastic model under the plane strain state.

The finite-element model has the same size as the standard specimen of the triaxial shear test, which is 39.1 mm × 80 mm (Fig. 13). The horizontal displacement at the top of the specimen is constrained, and the horizontal and vertical displacements at the bottom are constrained. The initial stress field of the model was reproduced by imposing a constant pressure in three directions. Then, a vertical displacement with a constant rate was imposed at the top. The soil parameters that are considered in the analysis are indicated in Table 4, and the characteristic length (refer to the previous study (Chen 2004a, b)) is assumed to be 0.001 m. The hardening modulus was deduced from the strain-softening entire-process curve (Fig. 12) as a dynamic changing value. A four-nodal-point element was adopted, and every nodal has three degrees of freedom: two displacement degrees of freedom and a plastic multiplier degree of freedom. The calculations were conducted considering a different number of elements (15 × 30 = 450, 20 × 40 = 800). The analysis was performed using the finite-element code ABAQUS (Hibbitt 2003).

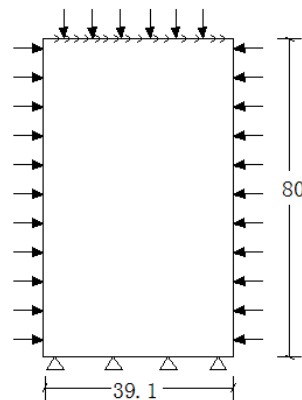


Fig. 13 Loading and boundary conditions in the finite-element analysis

Table 4 Soil parameters used in the analysis

$\gamma$ /kN/m <sup>3</sup>	$E$ /kPa	$\nu$	$c_p$ /kPa	$\varphi_p$ /°	$c_r$ /kPa	$\varphi_r$ /°	$l$ /m
20.8	30000	0.3	10	29.3	0	28	0.001

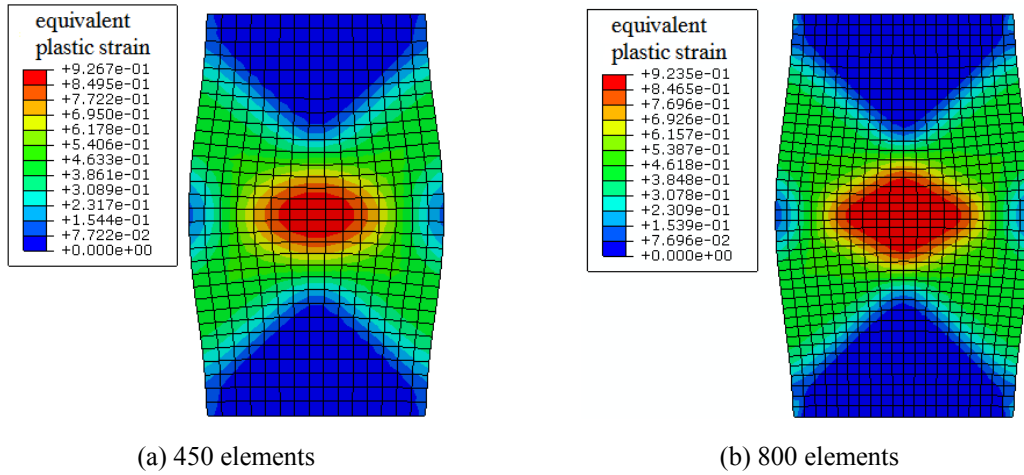


Fig. 14 Equivalent plastic strain field

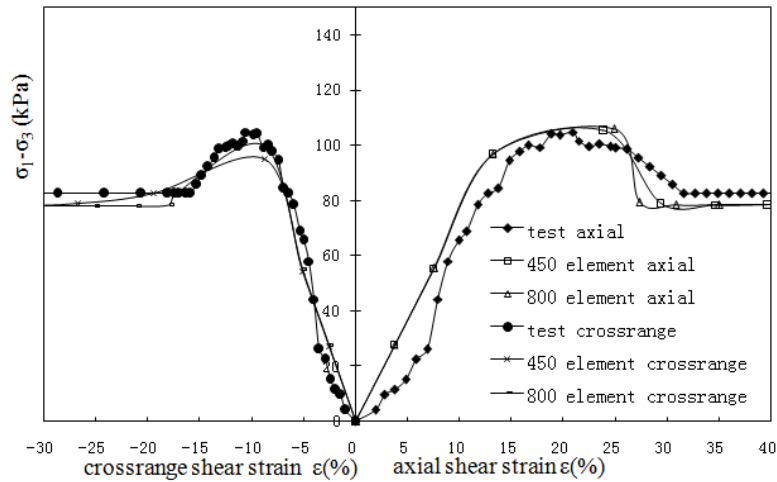


Fig. 15 Comparison of measured and computed curves

The calculated results from the models are compared in Figs. 14-15. The plastic strain field at the final step is presented in Fig. 14 in terms of the equivalent plastic strain. As observed, an intersection shaped stress concentrated zone was formed, and the shape and thickness of the shear zone with different mesh densities are almost identical, except the middle area of the zone is slightly different. Fig. 15 shows the deviator stress-strain curves in the shear zones, where the

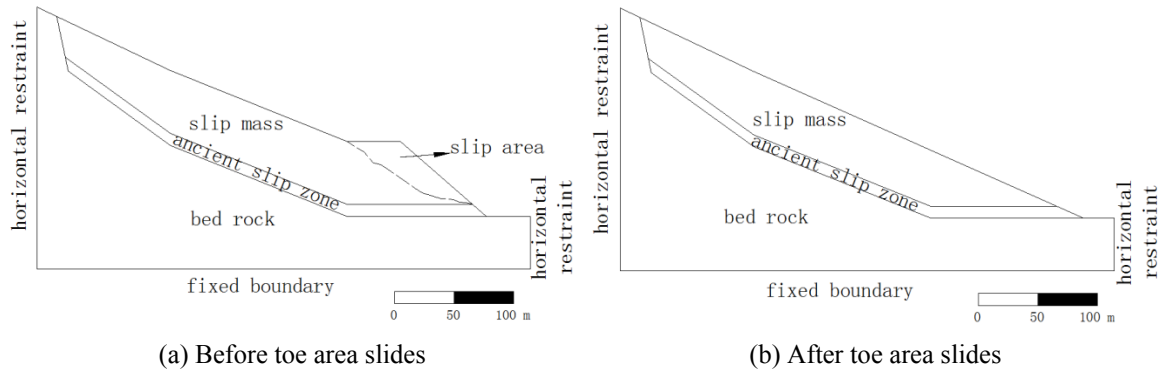


Fig. 16 Geometric model of the ancient landslide

deformation is concentrated. The curves of the gradient-dependent plastic soil model are notably close to the measured curve from the triaxial test. In addition, the ascent and residual stable stage of the two curves using the gradient-dependent plastic soil model with different mesh densities are notably close, whereas the middle stage is slightly different. Based on these analyses, it can be concluded that the numerical calculation using the gradient-dependent plastic soil model is not affected by the element number of the mesh.

#### 4. Numerical analysis of the ancient landslide

The ancient landslide geometry is demonstrated in Fig. 16(a), which is obtained based on the topographic section. It is approximately 500 m long and 200 m high, and a steep slope is formed at the toe of slope. Owing to the comprehensive effects of rainfall, river raised and excavation, the toe area slid (Fig. 16(a)). Because the stress field of the ancient landslide generates a re-distribution because of the slide of the toe area, the ancient landslide may reactivate. In this study, the effect of small-scale slide on the stability of the ancient landslide is analyzed. The analysis was performed using the finite-element code ABAQUS (Hibbitt 2003), and the simplified geometric model after the slide is shown in Fig. 16(b).

A stability analysis of the ancient landslide was first performed using the peak strength for the slip mass soil, ancient slip zone soil and bed rock before the toe area slides (Table 5). It is assumed that both soils and rock are described by an elastic plastic model with the Mohr-Coulomb failure criterion. The initial stress field of this ancient landslide was reproduced by progressively

Table 5 Parameters of soil and rock used in the analyses

	$\gamma$ /kN/m <sup>3</sup>	$E$ /kPa	$\nu$	$c_p$ /kPa	$\varphi_p$ /°	$c_r$ /kPa	$\varphi_r$ /°
Slip mass soil	21	40000	0.25	23	30	-	-
Slip zone soil	20.8	30000	0.3	10	29.3	0	28
Bed rock	27	1000000	0.25	150	35	-	-

increasing the gravity acceleration to  $9.8 \text{ m/s}^2$ . At the end of the gravity loading step, the resulting displacements and strains were reset to zero. Then, the sliding area was generally removed in the next step, and a re-distributional stress was generated. Using the peak strength parameters of the slip zone soils, the safety factor of the calculations in the step is 1.26 (obtained using a method based on a progressive reduction of the shear strength parameters). However, when the residual strength parameters of the slip zone soils are used, the calculation proves incompletely because of a lack of solution convergence. Therefore, the ancient landslide is considered unstable when the residual strength parameters of the slip zone soils are used, which implies that a progressive failure occurred with the operational strength along the slip zone that varied between the peak and residual strength values.

Finally, the landslide was analyzed considering the strain-softening behavior of the slip zone soil when the slip area is removed. The slip mass soils and the bed rock still exhibit elastic perfectly plastic behavior with the Mohr-Coulomb failure criterion. For the slip zone soils, a gradient-dependent plastic soil model that considered the strain-softening behavior was adopted. The strain-softening behavior of the slip zone soils was simulated by reducing the shear strength parameters from the peak strength to the residual strength with the increasing equivalent plastic strain as shown in Fig. 12. The characteristic length was assumed to be 0.1 m. The hardening modulus was deduced from the strength reduction curve (Fig. 12) at a dynamic changing value. Fig. 17 shows the mesh that was adopted before the slip occurred. A triangular gradient-dependent element of each node with three degrees of freedom was adopted. The slip zone where stress concentration is mostly likely to appear is more finely meshed.

Fig. 18 shows the displacement evolution that occurred during the progressive failure under the effect of the toe area slide. The displacement in Fig. 18 is an accumulated displacement, which reflects the sliding trend of the landslides. As observed, the slip mass soil and slip zone soil areas have an obvious displacement, whereas the bed rock is stable. The maximum displacement occurs at the toe of the landslide and can reach nearly 1 m. Fig. 19 shows the evolution of the equivalent plastic strains that occurred during the progressive failure. As observed, the strains are concentrated in the ancient slip zone and extend from the toe area of the slip zone to the top area, which finally causes the landslide to collapse when the concentrate area fills the entire ancient slip zone. Therefore, the numerical calculation that was performed using the gradient-dependent plastic soil model allows one to consistently predict the location and development of the plastic strains up to the complete failure. Based on the equivalent plastic strain that was calculated at the final

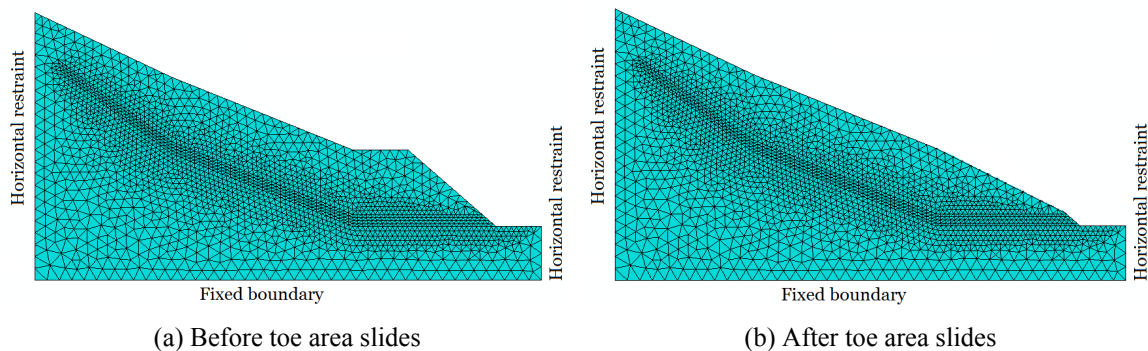


Fig. 17 Mesh and boundary conditions before the slip occurs

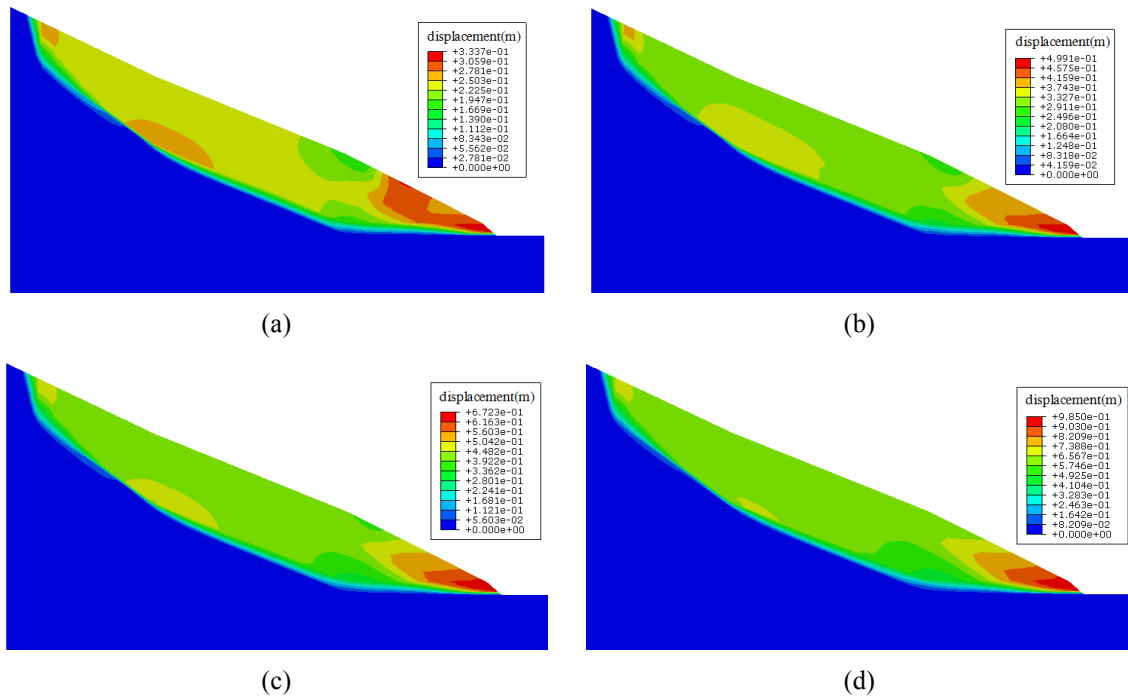


Fig. 18 Evolution of displacement under the effect of toe area slides

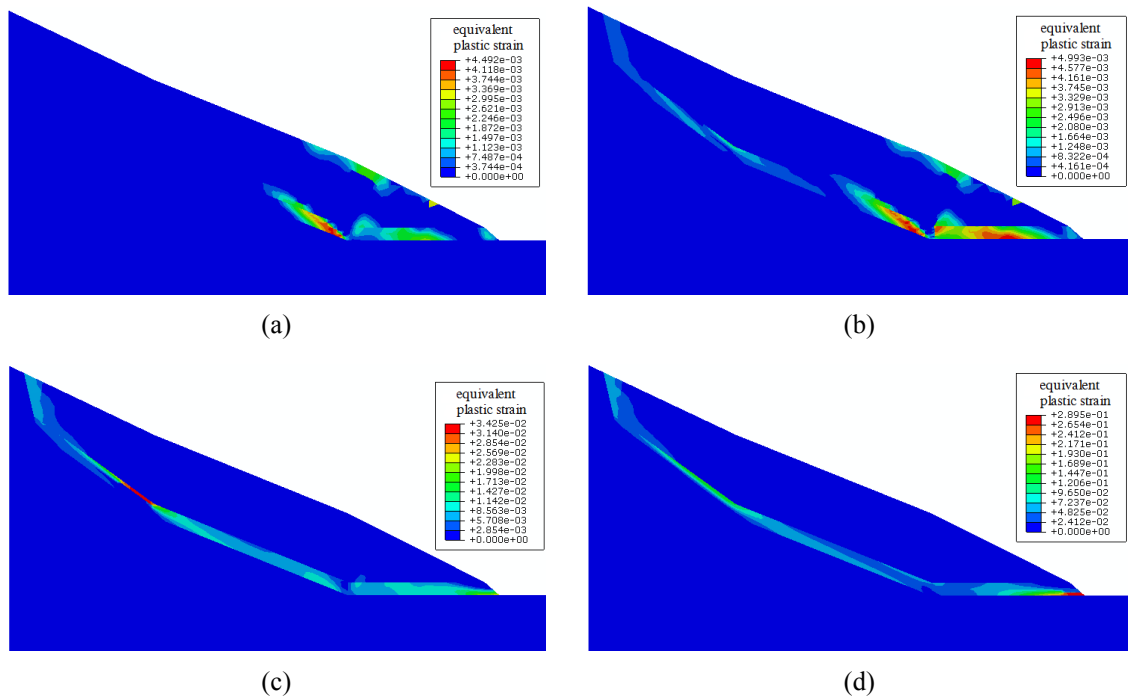


Fig. 19 Evolution of the equivalent plastic strain field

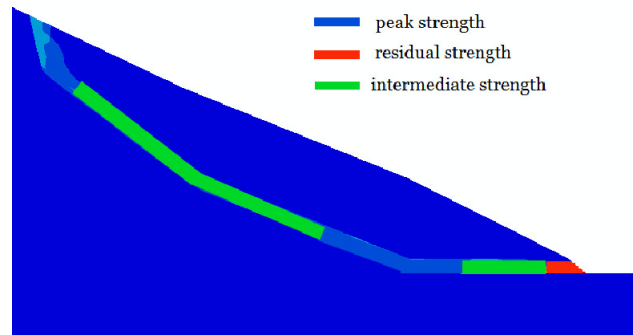


Fig. 20 Strength mobilized in the slip zone

step of the analysis, Fig. 20 shows the portions of the slip zone where the peak, residual or intermediate strength is mobilized. Considering the numerical calculation results that used the gradient-dependent plastic soil model with strain softening, the ancient landslide will reactivate because of the effect of the toe area slip. Therefore, some measures are suggested to prevent the reactivation of the ancient landslide, for example, using the anchor bolt to support the landslide.

## 5. Conclusions

Based on the Mohr-coulomb failure criterion, a gradient-dependent plastic model that considers the strain-softening behavior is presented in this study. The strain-softening characteristic of the soil was obtained from triaxial shear tests, which were performed on conventional specimens and pre-cut specimens from an ancient landslide zone. Based on the two test results, a method was proposed to combine the strain-softening of the entire process, and the dynamic variation rule of the soil strength parameters when the Mohr-coulomb strength criterion was obtained.

In the gradient-dependent plastic model, the strain-softening behavior of soils is simulated by reducing the shear strength parameters from the peak strength to the residual strength with the increasing equivalent plastic strain. In particular, the strength reduction depends on the hardening parameter and the Laplacian thereof, and the hardening modulus is obtained from the strength reduction curve as a dynamic changing value.

To assess the reliability of the model, some applications of the model have been performed. A series of triaxial shear tests were simulated using the gradient-dependent plastic model. The results show that the curves of the gradient-dependent plastic soil model are notably close to the measured curve of the triaxial test and are not affected by the element number of the mesh.

Finally, an approach to analyze the stability of an ancient landslide that was subject to toe area slip was performed in this study. The analysis showed that the toe area slip can trigger a progressive failure in soils with strain-softening behavior and cause the ancient landslide to reactivate.

## Acknowledgments

The project was supported by the National Natural Science Foundation of China (Grant No.

11072088 and Grant No. 41472279) and the Guangdong Provincial Water Resources Science & Technology Project (Grant No. ysk 2009-01).

## References

- Bjerrum, L. (1967), "Progressive failure in slopes of overconsolidated plastic clays and clay shales", *J. Soil Mech. Found. Div.*, **93**(5), 1-49.
- Brinkgreve, R.B.J. (1994), "Geomaterial models and numerical analysis of softening", Ph.D. Thesis, Delft University, Delft, The Netherlands.
- Chen, G. and Baker, G. (2004a), "Incompatible 4-node element for gradient-dependent plasticity", *Adv. Struct. Eng.*, **7**(2), 169-178.
- Chen, G. and Baker, G. (2004b), "Enhanced approach to consistency in gradient-dependent plasticity", *Adv. Struct. Eng.*, **7**(3), 279-284.
- Chen, Z., Morgenstern, N.R. and Chan, D.H. (1992), "Progressive failure of the Carsington Dam: a numerical study", *Can. Geotech. J.*, **29**(6), 971-988.
- Chen, X.P., Huang, J.W., Ng, C.W.W. and Ma, S.K. (2011a), "Centrifugal model tests on ancient bank landslide", *Chinese J. Geotech. Eng.*, **33**(10), 1496-1503.
- Chen, X.P., Huang, J.W., Yin, S.H. and Zheng, J.Z. (2011b), "Experimental study of strength property of slip zone soils", *Rock Soil Mech.*, **32**(11), 3212-3218.
- Chinese National Standard GB 50021-2001 (2001), Code for Investigation of Geotechnical Engineering, Beijing, China. [In Chinese]
- Conte, E., Silvestri, F. and Troncone, A. (2010), "Stability analysis of slopes in soils with strain-softening behavior", *Comput. Geotech.*, **37**(5), 710-722.
- Conte, E., Donato, A. and Troncone, A. (2013), "Progressive failure analysis of shallow foundations on soils with strain-softening behaviour", *Comput. Geotech.*, **54**, 117-124.
- De Brost, R. (1991), "Simulation of strain localization: A reappraisal of the Cosserat continuum", *Eng. Computation.*, **8**(4), 317-332.
- De Brost, R. (1992), "Gradient-dependent plasticity: formulation and algorithmic aspects", *Int. J. Numer. Method. Eng.*, **35**(3), 521-539.
- De Brost, R. and Sluys, L.J. (1991), "Localization in a Cosserat continuum under static and dynamic loading conditions", *Comput. Method. Appl. Mech. Eng.*, **90**(1), 805-827.
- De Brost, R. and Pamin, J. (1996), "Some novel development in finite element procedures for gradient-dependent plasticity", *Int. J. Numer. Method. Eng.*, **39**(14), 2477-2505.
- Di Prisco, C. and Imposimato, S. (2003), "Non local numerical analysis of strain localization in dense sand", *Mathematical and computer modeling*, **37**(5), 497-506.
- Di Prisco, C., Imposimato, S. and Aifantis, E.C. (2002), "A visco-plastic constitutive model for granular soils modified according to non-local and gradient approaches", *Int. J. Numer. Anal. Method. Geomech.*, **37**(5), 497-506.
- Dounias, G.T., Potts, D.M., and Vaughan, P.R. (1988), "Finite element analysis of progressive failure", *Comput. Geotech.*, **6**, 155-175.
- Georiadis, K., Potts, D.M. and Zdravkovic, L. (2004), "Modelling the shear strength of soils in the general stress space", *Comput. Geotech.*, **31**(5), 357-364.
- Han, J., Li, S.C., Li, S.C. and Yang, W.M. (2013), "A procedure of strain-softening model for elasto-plastic analysis of a circular opening considering elasto-plastic coupling", *Tunn. Undergr. Sp. Tech.*, **37**, 128-134.
- Hibbitt, K. (2003), "Getting started with ABAQUS Version 6.4", ANAQUUS Inc.
- Lars, P.M. and Stergios, G. (2009), "Suppressed plastic deformation at blunt crack-tips due to strain gradient effects", *Int. J. Solid. Struct.*, **46**(25-26), 4430-4436.
- Lu, Y. and Yang, W. (2013), "Analytical solutions of stress and displacement in strain softening rock mass

- around a newly formed cavity”, *J. Cent. South Univ. T.*, **20**(5), 1397-1404.
- Mohammadi, S. and Taiebat, H.A. (2013), “A large deformation analysis for the assessment of failure induced deformations of slopes in strain softening materials”, *Comput. Geotech.*, **49**, 279-288.
- Pietruszczak, S.T. and Mroz, Z. (1981), “Finite element analysis of deformation of strain-softening materials”, *Int. J. Numer. Method. Eng.*, **17**, 327-334.
- Potts, D.M., Dounias, G.T. and Vaughan, P.R. (1990), “Finite element analysis of progressive failure of Carsington embankment”, *Geotechnique*, **40**(1), 79-101.
- Simo, J.C. and Oliver, E.T. (1993), “An analysis of strong discontinuities induced by strain-softening in rate-independent inelastic solids”, *Comput. Mech.*, **12**(5), 277-296.
- Skempton, A.W. (1964), “Long term stability of clay slopes”, *Geotechnique*, **14**(2), 77-101.
- Troncone, A. (2005), “Numerical analysis of a landslide in soils with strain-softening behavior”, *Geotechnique*, **55**(8), 585-596.
- Wang, Z.M., Zhu, X.A., Tsai, C.T., Tham, C.L. and Beraun, J.E. (2004), “Hybrid-conventional finite element for gradient-dependent plasticity”, *Finite Elem. Anal. Des.*, **40**(15), 2085-2100.